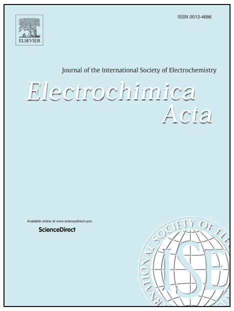

An investigation on the impact of halidization on substituted dimethoxybenzenes

Jeffrey A. Kowalski, Thomas J. Carney, Jinhua Huang, Lu Zhang, Fikile R. Brushett

PII: S0013-4686(19)32452-1
DOI: https://doi.org/10.1016/j.electacta.2019.135580
Reference: EA 135580

To appear in: *Electrochimica Acta*

Received Date: 13 February 2019
Revised Date: 21 December 2019
Accepted Date: 26 December 2019

Please cite this article as: J.A. Kowalski, T.J. Carney, J. Huang, L. Zhang, F.R. Brushett, An investigation on the impact of halidization on substituted dimethoxybenzenes, *Electrochimica Acta* (2020), doi: https://doi.org/10.1016/j.electacta.2019.135580.

CRedIT author statement

Jeffrey Kowalski: Methodology, Investigation, Validation, Formal analysis, Data Curation, Visualization, Writing – Original Draft, Writing – Review & Editing

Thomas Carney: Methodology, Formal analysis, Writing – Review & Editing

Jinhua Huang: Conceptualization, Resources

Lu Zhang: Conceptualization, Project administration, Writing – Review & Editing

Fikile Brushett: Conceptualization, Project administration, Supervision, Writing – Original Draft, Writing – Review & Editing

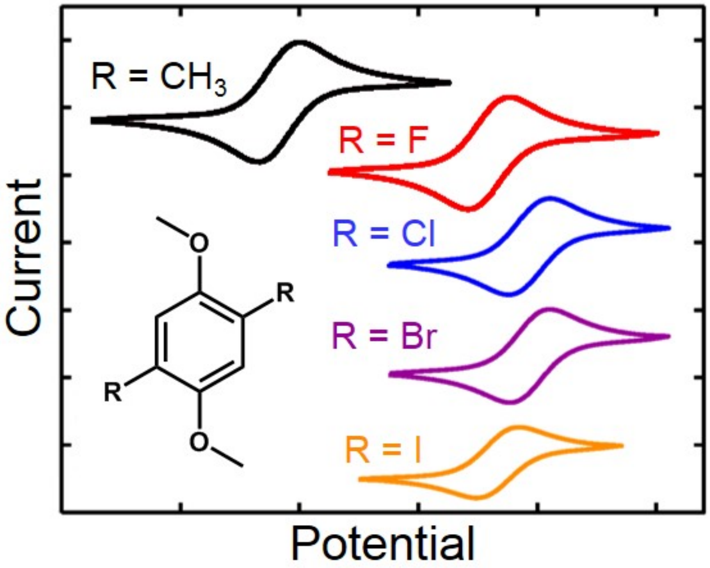
R = CH3
R = F
R = Cl
R = Br
R = I
R
R
O
O
Current
Potential

An investigation on the impact of halidization on substituted dimethoxybenzenes

Jeffrey A. Kowalski,[a,b] Thomas J. Carney,[a,c] Jinhua Huang,[d,e] Lu Zhang,[d,e] Fikile R. Brushett[a,b,*]

[a] Joint Center for Energy Storage Research, Massachusetts Institute of Technology, Cambridge, MA 02139, USA
[b] Department of Chemical Engineering, Massachusetts Institute of Technology, Cambridge, MA, 02139, USA
[c] Department of Materials Science and Engineering, Massachusetts Institute of Technology, Cambridge, MA, 02139, USA
[d] Joint Center for Energy Storage Research, Argonne National Laboratory, Lemont, IL 60439, USA
[e] Chemical Sciences and Engineering Division, Argonne National Laboratory, Lemont, IL 60439, USA
* Corresponding author: brushett@mit.edu

Abstract

Functionalized organic molecules are emerging as charge storage materials in electrochemical technologies as the breadth and diversity of the organic design space offers the possibility of purpose-built materials with property sets optimized for a particular application. First developed as overcharge protection materials in lithium-ion batteries, substituted dialkoxybenzenes represent a potentially promising molecular platform for advancing soluble charge storage materials. Here, we systematically substitute a series of halide groups at the 2- and 5-positions of the 1,4-dimethoxybenzene core, investigate the impact the halide groups have on molecular properties using electrochemical and spectroscopy methods, and compare these results to those of 2,5-dimethyl-1,4-dimethoxybenzene (25DDB), a previously reported derivative. In general, we observe that introduction of heavy halogen atoms leads to decreased gravimetric capacity as compared to 25DDB, but concomitantly improves solubility and redox potentials. As the halide functional group increases in size, the active material becomes less stable in its oxidized state as evinced by both cyclic voltammetry and bulk electrolysis cycling. None of the halogenated species are as stable as 25DDB indicating that these materials may be better suited for applications with more rapid cycling conditions (e.g., redox shuttling). More broadly, these results may serve as a useful data set for computational methods for materials discovery and optimization.

Keywords: electroactive organic, high potential, halidization, molecular engineering

Introduction

Electrochemical energy storage is a pivotal technology in modern society, underpinning the portable electronics revolution and enabling emergent efforts to decarbonize transportation and electricity generation [1–4]. While the optimal device configuration may vary, a ubiquitous feature is the reversible shuttling of electrons, over a range of timescales, through the oxidation and reduction of metal cations in the form of inorganic compounds, salts, and/or coordination complexes. However, for most of these chemistries, the degree to which electrochemical and physicochemical properties can be modified is limited, motivating exploration of alternate redox systems [5–8]. Recently, organic redox couples have enjoyed a renaissance spurred by the flexibility afforded by molecular functionalization and the potential for low-cost material synthesis [7,9–21]. The organic design space is rich and broad offering an elegant but complex toolbox for material design, which the community is only beginning to understand. In order to accelerate progress, computational methods such as genomic calculations [22], machine learning [23], and quantitative structure-property relations (QSPR) [24] are being utilized to augment traditional discovery approaches. Still, systematic experimental inputs are needed to inform and calibrate these tools (e.g., training sets).

While a number of molecular families have been examined including nitroxides [18,25,26], phenothiazines [12,27–31], cyclopropeniums [9,32,33], and isonicotinates [10,24], substituted dialkoxybenzenes are amongst the most well studied for electrochemical applications [11,34–42]. One particular dialkoxybenzene, 2,5-di-*tert*-butyl-1,4-bis(2-methoxyethoxy)benzene (DBBB), has been used and modified for several different applications including overcharge protection for lithium-ion batteries [38] and a redox active molecule for flow batteries [42]. Originally designed for overcharge protection due to its high redox potential and stability in nonaqueous electrochemical environments, DBBB has provided a promising platform for molecular engineering. To this end, efforts have been made to increase the solubility and to decrease the overall molecular weight. Huang *et al.* adjusted the length and symmetry of the ether chains on the 1- and 4-positions depressing the melting temperature such that several derivatives were liquid a room temperature, drastically increasing the solubility/miscibility in common nonaqueous electrolytes [11]. More recently, Huang *et al.* sought to identify a stable minimal structure, using DBBB as a starting materials, to increase atom economy and potentially reduce the active material cost by decreasing the number of synthesis steps [34]. That work lead to the development of 2,5-dimethyl-1,4-dimethoxybenzene (25DDB) where the *tert*-butyl groups, which provide steric protection for radical cation formed during oxidation, were replaced to methyl groups and the polyethylene glycol chains, which enable solubilization in polar electrolytes, were shortened to a single methoxy group. 25DDB showed similar stability and solubility to DBBB while doubling the gravimetric capacity.

Here, we seek to increase the redox potential of 25DDB to approach the upper stability limit of nonaqueous electrolytes, thus maximizing the available electrochemical window. Specifically, we substitute a series of halide groups (fluorine, chlorine, bromine, and iodine) onto the 25DDB structure on the 2- and 5-positions, in place of the methyl groups, and evaluate the effect on the physical and electrochemical properties of the molecule. Figure 1 shows the five molecules examined in this study: 25DDB, 2,5-difluoro-1,4-dimethoxybenzene (25FDB), 2,5-dichloro-1,4-dimethoxybenzene (25ClDB), 2,5-dibromo-1,4-dimethoxybenzene (25BrDB), and 2,5-diiodo-1,4-dimethoxybenzene (25IDB). While this work focuses on adjusting a single property (i.e., redox potential) with a goal of developing structure-property correlations for halides as functional groups on dialkoxybenzenes that may ultimately serve as inputs for future computational discovery tools [24], it also highlights some of the challenges in tuning specific property of a redox molecule without adversely impacting other properties.

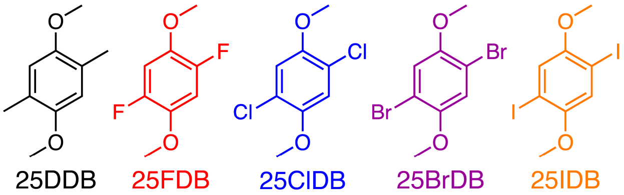

Figure 1: Chemical structures of 2,5-dimethyl-1,4-dimethoxybenzene (25DDB, black), 2,5-difluoro-1,4-dimethoxybenzene (25FDB, red), 2,5-dichloro-1,4-dimethoxybenzene (25ClDB, blue), 2,5-dibromo-1,4-dimethoxybenzene (25BrDB, purple), and 2,5-diiodo-1,4-dimethoxybenzene (25IDB, orange).

Experimental

Materials and Synthesis. Propylene carbonate (PC, anhydrous, 99.7%), ethylene carbonate (EC, anhydrous, 99%), dimethyl carbonate (DMC, anhydrous, ≥ 99%) and 1,2-dimethoxyethane (DME, anhydrous 99.5%) were purchased from Sigma Aldrich. Bis(trifluoromethane) sulfonimide lithium salt (LiTFSI, 99.9%) was purchased from BASF Corporation (Florham Park, NJ). All materials were stored in an argon-filled glovebox (MBraun Labmaster, $O_2 < 1$ ppm, $H_2O < 5$ ppm). Prior to use, all solvents were dried over activated molecular sieves (3 Å beads, Fluka) for at least 24 h.

2,5-dimethyl-1,4-dimethyoxybenzene (25DDB) was synthesized in house at Argonne National Laboratory following a modified procedure previously reported [34]. In brief, sodium borohydride ($NaBH_4$, 7.57 g, 0.200 mol, Sigma-Aldrich, ≥ 96%) was added dropwise to a solution of 2,5-dimethyl-1,4-benzoquinone (13.62 g, 0.100 mol, Sigma-Aldrich, ≥ 98.0%) in ethanol (100 mL, ACROS, 99.5%) and water (100 mL) under nitrogen. The reaction was stirred for 30 min at room temperature. A solution of potassium hydroxide (40 mL, 10 M, 0.400 mol, Sigma-Aldrich, ≥ 85%) was then added, and the resulting mixture was stirred for another 30 min and was heated under reflux. Dimethyl sulfate (37.85 mL, 0.400 mol, Sigma-Aldrich, ≥ 99.8%) was added dropwise. The resulting mixture was stirred under reflux for 12 h before being cooled to room temperature and extracted with ethyl acetate (Sigma-Aldrich, 99.8%). The combined organic layers were washed with water and dried over Na_2SO_4 (Sigma-Aldrich, ≥ 99.0%). After being concentrated in vacuo, the residue was purified by flash column chromatography (silica gel, eluted with ethyl acetate / hexanes, (Sigma-Aldrich, ≥ 98.5%) = 1/10) to yield the product (14.57 g, 88%) as a white solid. ^{1}H NMR (500 MHz, $CDCl_3$) δ 6.68 (s, 2H), 3.80 (s, 6H), 2.23 (s, 6H) (Figure S1); ^{13}C NMR (125 MHz, $CDCl_3$) δ 151.4, 124.3, 113.7, 56.1, 16.1 (Figure S2). 2,5-difluoro-1,4-dimethyoxybenzene (25FDB, Sigma-Aldrich, 99%), 2,5-dichloro-1,4-dimethyoxybenzene (25ClDB, Sigma-Aldrich, ≥ 98.0%), 2,5-dibromo-1,4-dimethyoxybenzene (25BrDB, Sigma-Aldrich, 97%), 2,5-diiodo-1,4-dimethyoxybenzene (25IDB, Oakwood Chemical, 95%) were used as received.

Electrolyte preparation and viscosity measurements. All electrolyte formulations and subsequent experiments were performed in an argon-filled glove box at ca. 29 °C. All electrolytes were prepared in volumetric flasks to account for the volume change associated with the high concentration of supporting salt and active material. Electrolyte viscosity was measured using a vibrational viscometer probe (Viscolite V-700, ± 0.1 cP accuracy) and electrolyte density was determined using an analytical balance (Metler-Toledo XP105, ± 0.1 mg accuracy) and a known electrolyte volume.

Voltammetry. Cyclic voltammetry (CV) was performed in a three-electrode electrochemical cell with a 3 mm diameter glassy carbon disk electrode (CH Instruments) or an 11 ± 2 μm diameter carbon fiber microelectrode (UME, CH Instruments) as the working electrode, a gold coil counter electrode (CH Instruments), and fritted lithium foil (99.9%, Alfa Aesar) as the reference electrode. Before each measurement, the working electrodes were polished on a MicroCloth pad with 0.05 μm alumina powder (Buehler Ltd.), rinsed with deionized water (Millipore), and wiped dry with lens paper (VWR). Before being placed in the fritted tube with a 1 M LiTFSI in PC fill solution, the lithium reference electrode was scraped with polypropylene to clean the metal surface. For the disk electrode experiments, all data was collected using a Bio-Logic VSP-300 potentiostat, applying 100% automated *i*R compensation. The resistance measured for each experiment was about 100 Ω, which corresponds to a correction of ca. 10 mV at the highest currents. The scan rates used were 10, 20, 30, 40, 50, 75, and 100 mV/s.

The disk electrode experiments were used to calculate the redox potential, peak separation (reversibility), and diffusion coefficient. The redox potential was calculated by taking the average of the anodic and cathodic peak potentials while peak separation was determined by taking the difference between these two peak potentials. The diffusion coefficient for the neutral species was estimated using the Randles-Sevcik equation:

$$i_p = 0.4463nFAC\left(\frac{nFD}{RT}\nu\right)^{0.5} \qquad \text{Equation 1}$$

where i_p is the peak current (A), n is the number of electrons transferred (n = 1), F is the Faraday constant (96485 C/mol e^-), A is the electrode area (0.0707 cm^2), C is the bulk concentration (1×10^{-5} mol/cm^3), R is the universal gas constant (8.314 J/mol-K), T is the absolute temperature (302.15 K), D is the diffusion coefficient (cm^2/s), and ν is the scan rate (V/s). The peak current was obtained by using the peak current from the cyclic voltammogram and subtracting an extrapolated background current [34].

All data using the UME was collected with a 630E potentiostat (CH Instruments, Inc.) at a scan rate of 10 mV/s. The steady-state currents were obtained from the UME voltammetry to estimate the active species concentration in solution:

$$i_{ss} = 4nFrDC \qquad \text{Equation 2}$$

Where i_{ss} is the steady state current obtained at high overpotentials (A), n is the number of electrons transferred (n = 1), F is the Faraday constant (96485 C/mol e^-), r is the UME radius (5.5×10^{-4} cm), C is the bulk concentration (mol/cm^3), and D is the diffusion coefficient (cm^2/s).

Bulk electrolysis. Extending cycling experiments were performed in a commercial bulk electrolysis cell (BASi) controlled by the VSP-300 potentiostat (Bio-Logic). The working, counter, and reference electrodes were reticulated vitreous carbon (BASi), lithium foil (Alfa Aesar), and fritted lithium foil (Alfa Aesar), respectively. All extended cycling experiments used 30 mL of 1 M LiTFSI in a 1:1 by weight mixture of EC:DMC with 0.001 M active species and were stirred at a rate of 900 rpm. The current for the galvanostatic cycling was set to 0.402 mA (equivalent to a 0.5 C rate) and the solutions were charged between 0 and 50% state of charge (SOC). Each solution was charged and discharged for 1 h each or until a predetermined potential cutoff was reached (150 mV above and below the corresponding peak potentials obtained from CV), whichever occurred first. The potential cutoff was set in order to avoid accessing additional irreversible faradaic reactions involving either the active material or the supporting electrolyte.

Decay analysis of the 25FDB was performed at higher active species concentration and thus a custom H-cell with a higher surface area-to-volume ratio for electrolysis experiments was used. A similar configuration has been described in previous reports [24,27,43]. The cell consisted of two electrolyte chambers (3.5 mL), separated by an ultra-fine glass frit (P5, Adams and Chittenden) to minimize crossover. In these experiments, 3.5 mL of 0.01 M active species in 1 M LiTFSI was loaded into each side of the cell. Both chambers were stirred continuously during cycling experiments (1400 rpm). Two reticulated vitreous carbon electrodes (ERG Aerospace Corp.), one in each chamber, were used as the working and counter electrodes with a fritted lithium foil (Alfa Aesar) reference electrode housed in the working electrode chamber. These experiments sought to access the full SOC range (0 – 100%) thus potential cutoffs were set 0.25 V above and below the redox potential to charge and discharge the working solution. The current was set to 0.938 mA such that the theoretical charging and discharging times were 1 h each (equivalent to a 1 C rate). CV was performed before cycling and after each cycle using a 3 mm glassy carbon electrode inserted into the bulk electrolysis working electrode chamber. Reticulated vitreous carbon and fritted lithium foil served as the counter electrode and the reference electrode, respectively. Liquid phase nuclear magnetic resonance (NMR) experiments were conducted at room temperature using a Bruker Avance-400 NMR Spectrometer. Prior to NMR analysis, all solutions were mixed in a 1:1 ratio with deuterated dimethyl sulfoxide (99.9 atom % D, anhydrous, Aldrich).

Solvated Diameter. The Stokes-Einstein equation was used to experimentally estimate the solvated diameter of the active species:

$$D = \frac{kT}{6\pi\mu r} \quad \text{Equation 3}$$

Where D is the diffusion coefficient (m^2/s), k is the Boltzmann constant (1.38×10^{-23} J/K), T is the absolute temperature (K), μ is the dynamic viscosity (kg/m-s), and r is the Stokes radius (m). The diffusion coefficient was previous determined using the Randles-Sevcik analysis (Equation 1). The viscosity of the supporting electrolyte (solvent and 1 M supporting salt) was used as it was assumed that a 0.010 M concentration of active species would have a negligible contribution on the solution viscosity.

Computation. The molecular diameter was calculated using Chem3D Pro. The optimal structure was calculated using MM2 energy minimization. The distance between the centers of the atoms was then calculated using the Cartesian coordinates provided by the Chem3D Pro. For each of the structures, the Van der Waals diameter [44] (for hydrogen, fluorine, chlorine, bromine, and iodine) was added to the calculated distance in order to account for the additional radius of each of the molecules. Density functional theory (DFT) was used to calculate the wave functions and bond lengths for each active material using B3LYP with a basis of 6-31+G(d) in a polarizable continuum model of water. The iodine-substituted species could not be computed accurately because of the large number of electrons.

Results and Discussion

The electrochemical properties and cycle stability of a series of halide substituted 1,4-dimethoxybenzenes (25FDB, 25ClDB, 25BrDB, and 25IDB) are measured using voltammetric and electrolytic techniques in combination with density functional theory (DFT) analysis and nuclear magnetic resonance spectroscopy (NMR). The characteristics of these molecules are compared to each other as well as to 25DDB to correlate trends in performance-relevant properties with molecular structure.

Voltammetric analysis

Cyclic voltammetry (CV) measurements were performed to determine the redox potential, reversibility (chemical and electrochemical), and diffusion coefficient of each compound. In all experiments, the active species were dissolved in a supporting electrolyte consisting of 1 M lithium bis(trifluoromethane)sulfonimide (LiTFSI) in either propylene carbonate (PC, background scan, Figure S3) or 1,2-dimethoxyethane (DME, background scan, Figure S3). PC was initially selected as a solvent due to its wide electrochemical stability window and low volatility; however, as 25IDB was found to be insoluble in the PC-based electrolyte, DME was also used as a solvent. Figure 2 shows cyclic voltammograms of all compounds in 1 M LiTFSI in DME (solid lines) and 1 M LiTFSI in PC (dashed lines).

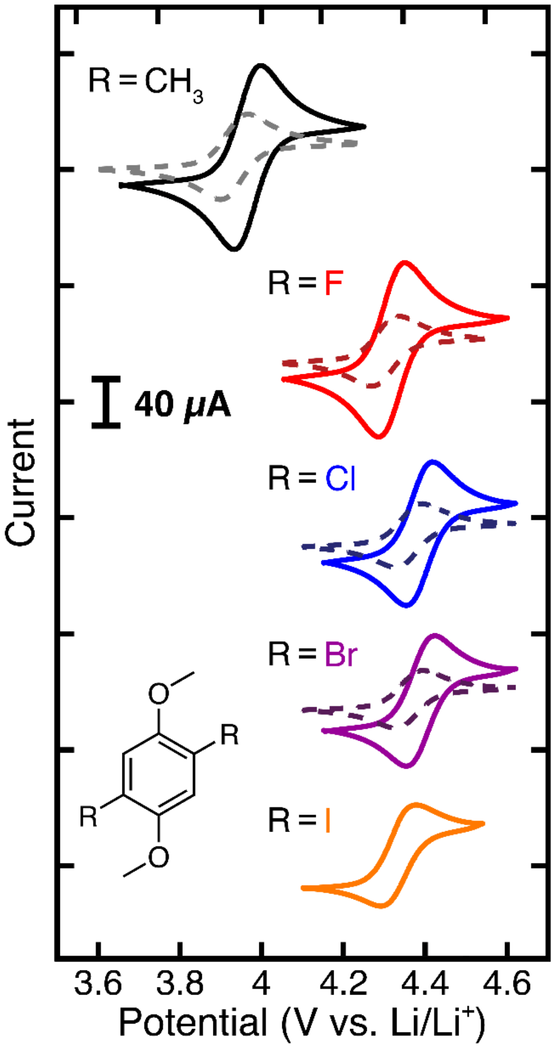

Figure 2: Cyclic voltammograms from top to bottom of 25DDB (black, gray), 25FDB (red), 25ClDB (blue), 25BrDB (purple), and 25IDB (orange). The solid and dashed lines correspond to

supporting electrolytes of 1 M LiTFSI in DME and 1 M LiTFSI in PC, respectively. All data was collected with a scan rate of 20 mV/s with 0.01 M active species. The working, counter, and reference electrodes used were a 3 mm glassy carbon disk, a gold coil, and a fritted lithium foil.

Based on the analysis of the CVs, electrochemical and transport properties can be extracted (Table 1). As expected, each of the halide derivatives has a redox potential 300 – 400 mV more positive than that of 25DDB as the more electron-withdrawing halides lower the electron density around the aromatic core, resulting in a greater ionization potential (calculated by DFT, Table 1) and, consequently, an increased oxidation potential. As weak electron-withdrawing substituents, halides impart both induction and resonance effects which manifest as electron-withdrawing and electron-donating behaviors, respectively. Therefore, though fluorine is the most electronegative substituent, due to its strong resonance effect, 25FDB does not afford the highest potential, but rather the lowest of the halide-substituted molecules. 25BrDB demonstrates the highest redox potential in both electrolytes, followed by 25ClDB, 25IDB, and then 25FDB in agreement with the Hammett sigma constants for the substituent groups [45,46]. We note the slight offset (15 – 30 mV) in redox potential across all tested species in the two electrolytes, which we attribute to a combination of different junction potentials between the electrolyte solution and the reference electrode as well as different interactions between the electrolyte solution and the solubilized redox molecules.

Analyses of the oxidative and reductive peaks of the CV, as a function of scan rate and electrolyte composition, provide insight into the stability of the charged species, as well as the kinetic and transport characteristics of the redox species. Of the halide-substituted molecules, 25FDB has the smallest peak separation of 61.0 ± 0.6 mV at a scan rate of 10 mV/s, with peak separation increasing with increasing halide size (Table 1). Over all of the scan rates tested, the peak separation for each molecule only increases by about 2 mV from scan rates of 10 to 100 mV/s after 100% *i*R compensation; the slight increase in the peak separation indicates that the electrochemical reactions are quasi-reversible, but still have relatively large kinetic rate constants, that could not be resolved by the techniques used in this work. Further, as the halide becomes larger, the peak current ratio increasingly deviates from unity, signifying that either the oxidized species is less stable for the larger halogenated species or oxidative electrolyte decomposition is convoluting the electrochemistry at these high potentials. As all of the halogenated species have a similar redox potential and the electrolyte background scans (Figure S3) do not show a significant current at these potentials, it appears more likely that the derivatives with the large halide groups are reacting with the electrolyte, reducing the oxidative stability. As expected the diffusion coefficient, as determined by Randles-Sevcik analysis, decreases as the substituted halide size, and thus Stokes radius, increase (Table 1).

Table 1: A summary of electrochemical and transport properties of 25DDB, 25FDB, 25ClDB, 25BrDB, and 25IDB as determined from CV experiments performed in 1.0 M LiTFSI in PC (top) and 1.0 M LiTFSI in DME (*bottom*), and the ionization potential determined by DFT. All electrochemical experiments were performed in triplicate.

	25DDB	25FDB	25ClDB	25BrDB	25IDB
Redox Potential (V vs. Li/Li$^+$)	3.930 ± 0.001	4.301 ± 0.001	4.359 ± 0.001	4.361 ± 0.001	—
	3.964 ±0.001	*4.318 ±0.001*	*4.386 ±0.001*	*4.388 ±0.001*	*4.332 ±0.001*
Ionization Potential (eV)	5.447	5.643	5.663	5.654	—
Peak Separation (mV)	60.3 ± 0.7	61.0 ± 0.6	61 ± 1	61.7 ± 0.9	—
	62.2 ±0.3	*60.3 ±0.3*	*62.7 ±0.9*	*65 ±2*	*80 ±5*
Peak Current Ratio ($I_{p,o}$ / $I_{p,r}$)	1.003 ± 0.002	1.03 ± 0.01	1.04 ± 0.02	1.08 ± 0.03	—
	1.01 ± 0.01	*1.01 ± 0.01*	*1.05 ± 0.01*	*1.06 ± 0.03*	*1.17 ± 0.05*
Diffusivity (× 10^{-6} cm^2/s)	2.4 ± 0.1	1.6 ± 0.1	1.4 ± 0.1	1.3 ± 0.1	—
	12.0 ±0.4	*8.6 ±0.9*	*7.6 ±0.2*	*7.1 ±0.1*	*5.5 ±0.2*

Upon examining the effective solvated diameter via the Stokes-Einstein relationship (solution viscosities: 8.5 cP in 1 M LiTFSI in PC and 1.3 cP in 1 M LiTFSI in DME), the solvated diameters for the halide-substituted compounds appear larger than expected suggesting complexation between the active species and electrolyte (Table 2). The lone electron pairs on the halides can be incorporated into conjugation, resulting in enhanced electron density, which, in turn, can complex with Li cations in the supporting salt, increasing the effective solvated diameter [47]. Weaker intermolecular interactions are anticipated for methylated compounds leading to a smaller solvation diameter [48]. This becomes particularly evident when comparing the ratio of the effective solvated diameter to the molecular diameter, as calculated from the energy minimization of the structure, across the series in both supporting electrolytes. Larger solvated diameters are observed in the DME-based electrolyte as compared to the PC-based electrolyte which we hypothesize is due to differences in the solvent structure. Specifically, DME has many freely rotating bonds whereas PC has a more rigid ring structure, thus DME can more easily coordinate with the redox active species and itself [47].

The active species solubility of both the oxidized and neutral species is another important property for achieving high-capacity charge-storage solutions. Unfortunately, each oxidized species could not be isolated, and therefore the solubility could not be measured. UV-Vis did not yield a linear signal for the neutral halogenated structures at low concentrations (0.1 mM – 30 mM), as would be expected from Beer's Law. Therefore, solubility was estimated using a combination of electrochemical techniques. First, a saturated solution of the active material was made by adding an excess of active material to 3 mL of electrolyte and allowing the solution to equilibrate for 48 h. The supernatant was then probed via microelectrode voltammetry where the measured steady-state current was used to estimate a saturation concentration (Figure S9). Note that this calculation requires knowledge of the active species diffusion coefficient which can vary as a function of concentration [49–51]. For the initial measurement, we assume that the diffusion coefficient measured under dilute conditions (see Table 1) is a sufficient representation. To validate this assumption, the saturated solution was diluted by a known amount, based on the previously estimated concentration, and Randles-Sevcik analysis was employed to provide a second estimate of the saturation concentration. In greater detail, the saturated solutions are diluted to a concentration between 0.005 and 0.010 M, and CV measurements are performed, over a range of scan rates to generate a Randles-Sevcik plot, from which an "actual" concentration can be determined, again based on the knowledge of the diffusion coefficient which was previously determined in a similar concentration regime. By multiplying this "actual" concentration by the dilution factor, a more accurate estimate of saturation concentration can be obtained (Table 2). We note that all of the refined estimates were within 5% of the initial estimate from the microelectrode, which is consistent as the overall solubilities of the compounds were not high enough to significantly impact the solution viscosity or the intermolecular interactions. When the increase in supporting salt concentration is accounted for, the determined solubility of 25DDB is in agreement with prior literature in PC [34].

In agreement with prior reports, the solubility of all of the species is greater in the DME-based electrolytes than in the PC-based electrolytes [52,53]. In general, as the halide substituent becomes larger, the solubility decreases in both electrolytes as larger local dipoles exist with smaller halides, due to increased electronegativity, which increases the solubility in polar solvents. The polarity of the C-F, C-Cl, C-Br, and C-I bonds are 1.43, 0.61, 0.41, and 0.11, respectively [44]. Additionally, the solubility of 25FDB is greater than that of 25DDB due to its smaller size and the greater electronegativity of the substituent groups [54].

Table 2: A summary of physical properties of 25DDB, 25FDB, 25ClDB, 25BrDB, and 25IDB in 1 M LiTFSI in PC (top) and 1 M LiTFSI in DME (*bottom*).

	25DDB	25FDB	25ClDB	25BrDB	25IDB
Molecular Diameter (Å)	9.1	8.4	9.7	10.2	11.0
Effective Solvated Diameter (Å)	21 ± 1 *28 ±1*	32 ± 1 *40 ±4*	36 ± 2 *44 ±1*	41 ± 2 *48 ±1*	— *62 ±2*
Solubility (mol/L)	0.10 *0.35*	0.19 *0.42*	0.10 *0.27*	0.05 *0.18*	Insol. *0.03*

Electrolytic analysis

Bulk electrolysis cycling was performed to investigate the cyclability of the halogenated compounds over longer time periods (~ 1 day). For these experiments, the electrolyte composition was changed to 1 M LiTFSI in a binary solvent mixture of ethylene carbonate (EC) and dimethyl carbonate (DMC) in a 1:1 weight ratio (background scan, Figure S3). This electrolyte was selected in an attempt to reduce the presence of asymmetric background processes that convolute analyses of the charge storage efficiency and species decomposition, which are present, to a greater extent, in both PC and DME (Figure S3). All redox species exhibit similar voltammetric and solubility behavior in the mixed carbonate electrolyte as compared to in the PC electrolyte, including the insolubility of 25IDB. Therefore, all active materials except 25IDB were tested at 0.001 M in 30 mL of solution with a current of 0.402 mA (0.5 C) and charged to 50% SOC. Figure 3 shows the voltage profiles for cycles 2 to 6 for each compound tested with a full set of voltage profiles (20 cycles) available in the supporting information (Figures S10-S13).

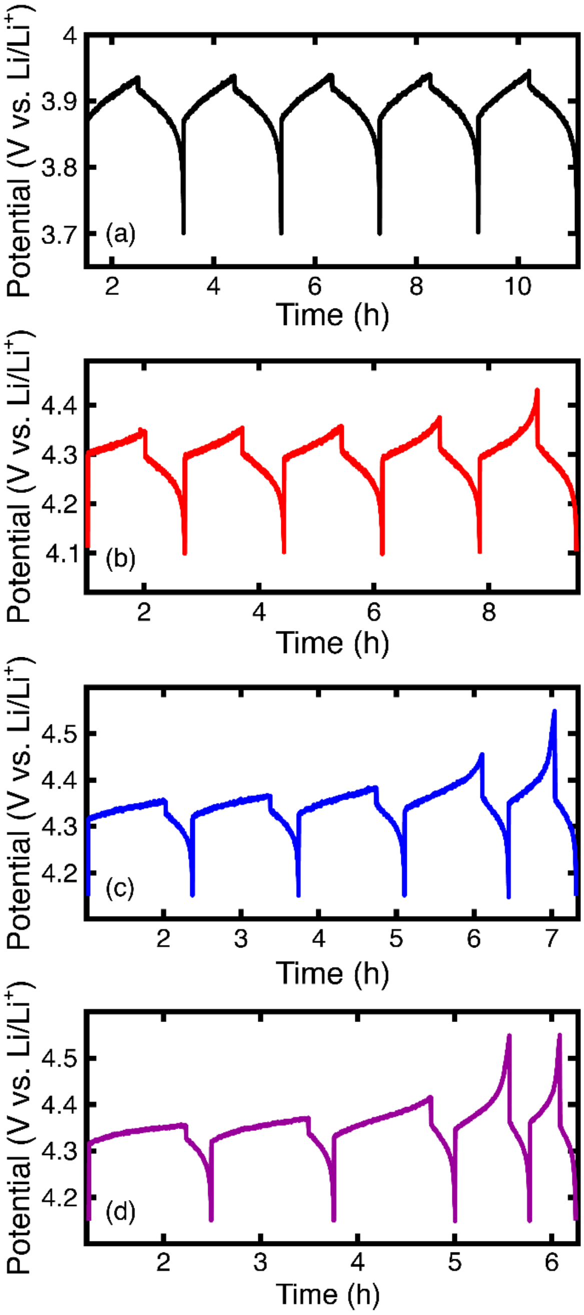

Figure 3: Bulk electrolysis voltage profiles for the second through sixth cycles of 0.001 M 25DDB (a), 25FDB (b), 25ClDB (c), and 25BrDB (d) each in 1 M LiTFSI in 1:1 weight ratio of EC:DMC. The charge/discharge current was 0.402 mA (0.5 C). 25IDB was not insoluble in this electrolyte solution.

From the 2nd to 6th cycles, a trend of the stability can be inferred because the potential cutoff for all halogenated compounds is reached whereas the 25DDB molecule always reaches the time cutoff. This trend is confirmed by examining the charging capacity as a function of cycle number (Figure 4) because as the halide substituent becomes larger, the faster the capacity fades. The coulombic efficiency of the cycles that reach the time cutoff further support the decomposition trend (Figure S14). The average coulombic efficiency of 25FDB, 25ClDB, and 25BrDB is 65%, 33%, and 26%, respectively. When compared to the coulombic efficiency of the 25DDB (96%), it is consistent that the halide substituted species are much less stable than 25DDB, and as the substituted halide becomes larger, the charged species becomes less stable. Because the coulombic efficiencies are so low and the cycling lifetime is short, it is likely that the charged active material decays to a new species which is not redox active in the potential window used in these experiments. Note that the first bulk electrolysis cycle is not shown here as it does not display representative charging/discharging behavior. This is an artifact of cycling between 0 and 50% state-of-charge, a range that was chosen to enable comparison with prior work on substituted dialkoxybenzenes [11,34]. Specifically, the first cycle represents a preconditioning of the solution and electrodes. This generally leads to a full charging cycle and a very limited discharging cycle, and thus, a poor coulombic efficiency. The first cycle is shown in the full cycling profiles (Figures S10-S13).

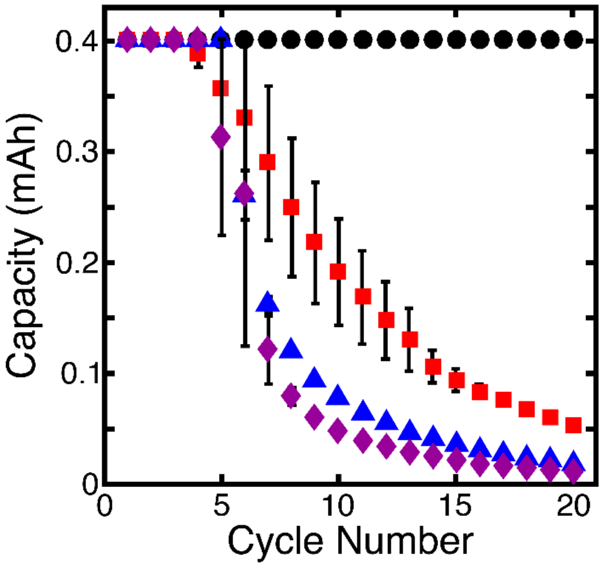

Figure 4: Bulk electrolysis charging capacity of 0.001 M of 25DDB (black, circles), 25FDB (red, squares), 25CIDB (blue, triangles), and 25BrDB (purple, diamonds) each in 1 M LiTFSI in 1:1 EC:DMC. All experiments were conducted in duplicate. 25IDB was not insoluble in this electrolyte solution.

Decay Characterization

To better understand the decay behavior observed in Figure 4, particularly the halide dependence, DFT calculations were performed on 25DDB, 25FDB, 25ClDB, and 25BrDB. The highest occupied molecular orbital (HOMO) was examined for both the neutral and oxidized species (Figure S15). As expected, as the halide size and therefore the overall number of associated electrons increases, the electron density around the halide increases for both the neutral and oxidized species, making it a better leaving group. Thus, we hypothesize that the increased capacity fade with larger halide size is due to the halide breaking off from the charged redox species through solvent attack [55,56].

Both ^{1}H NMR and ^{19}F NMR were performed on 25FDB before cycling and after the capacity faded below 1% of the initial capacity (20 cycles, Figure S16) with major peak locations summarized in Table 3. Here, to improve the NMR signal, the active species concentration was increased to 0.010 M. Additionally, the solvent was switched to PC from the mixed carbonate solvent in order to reduce the number of compounds in solution. In this case, because 25FDB has the lowest redox potential of the substituted halides, the higher potential electrolyte was also not as necessary. During cycling in the PC based electrolyte, a similar decay rate was observed for 25FDB as in the mixed carbonate system (Figure S11 and Figure S16). In the ^{19}F NMR, the only peaks present before cycling corresponded to the 25FDB parent molecule (Figure 5a) and the TFSI^{-} anion in the supporting salt (LiTFSI, Figure S17 and Figure S18). After cycling, the only peaks that remain are from the TFSI^{-} anion (Figure 5a, Figure S17 and Figure S18). Consistent with the ^{19}F NMR, the ^{1}H NMR data (Figure 5b) showed decay of the 25FDB species but also provides a clear indication of the decay mechanism complexity. Quantitative analysis of these emergent features is beyond the scope of the present work, especially considering critical fine details are likely to be masked by the strong PC solvent signal (Figure S17 and Figure S18). Note that Figure 5 only highlights where non-solvent peaks appeared or disappeared over the full range shown in the background scans (Figure S17 and Figure S18).

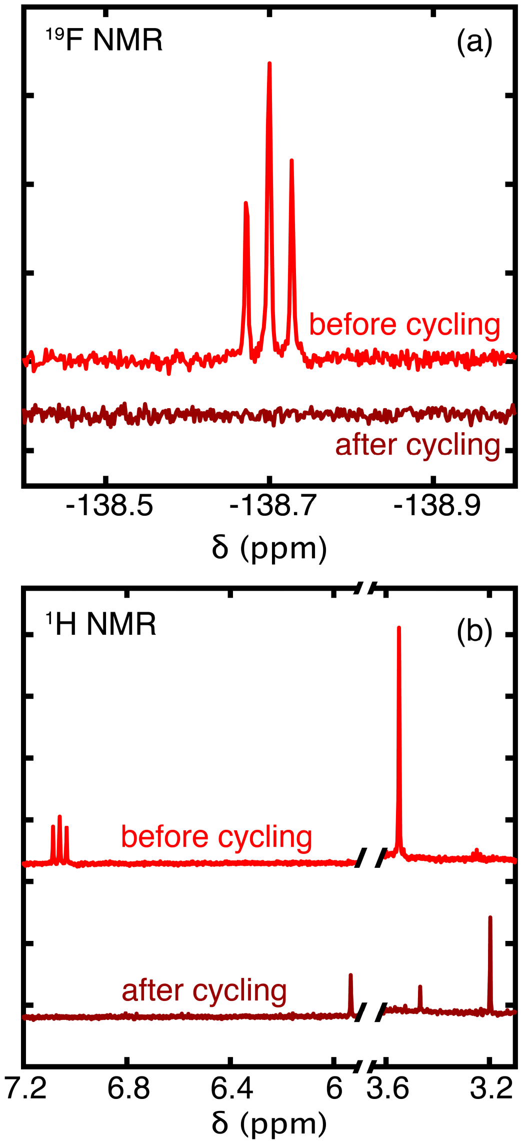

Figure 5: The ^{19}F NMR (a) and ^{1}H NMR (b) both before cycling (red) and after cycling (dark red) for 0.010 M 25FDB in 1 M LiTFSI in PC.

Taken together, these NMR spectra suggest that the decomposition process involves the halide leaving the molecule due to the disappearance of the fluorine peaks in ^{19}F NMR and the triplet corresponding to the benzene in ^{1}H NMR. As no additional fluorine peaks are observed by NMR we hypothesize that any free fluoride anions rapidly complex with excess lithium cations, present in the supporting electrolyte, and precipitate as lithium fluoride (LiF). However, LiF was not isolated from the electrolyte due to the low active material concentration, and the low solubility of LiF in PC [57].

Table 3: Summary of the major NMR peaks before and after cycling. Note that the solvent and supporting salt peaks are omitted from this table (See Figure S17 and Figure S18 for background NMR scans).

	^{1}H NMR	^{19}F NMR
Before cycling	3.55 (s), 7.06 (dd) J = 10.5	-138.7 (t) J = 10.1
After cycling	3.19 (s), 3.47 (s), 4.48 (s), 5.93 (s)	None

In an effort to better understand the decay processes, bulk electrolysis was combined with voltammetry to evaluate the evolution in the CV profile of 25FDB as a function of charge/discharge cycling. Overall, 25FDB was cycled to 100% state-of-charge for a total of 10 cycles (Figure 6a). The charging capacity (Figure 6b) was monitored and CV scans from 1.5 to 4.55 V vs. Li/Li^{+}, were taken before testing and then after every charge/discharge cycle for 10 cycles (Figure S19). Finally, the solution was allowed to rest for 10 h, with all of the electrodes removed from the solution, after which a final CV was performed to determine if chemical processes continue in the absence of electrochemical stimulus (Figure 6c).

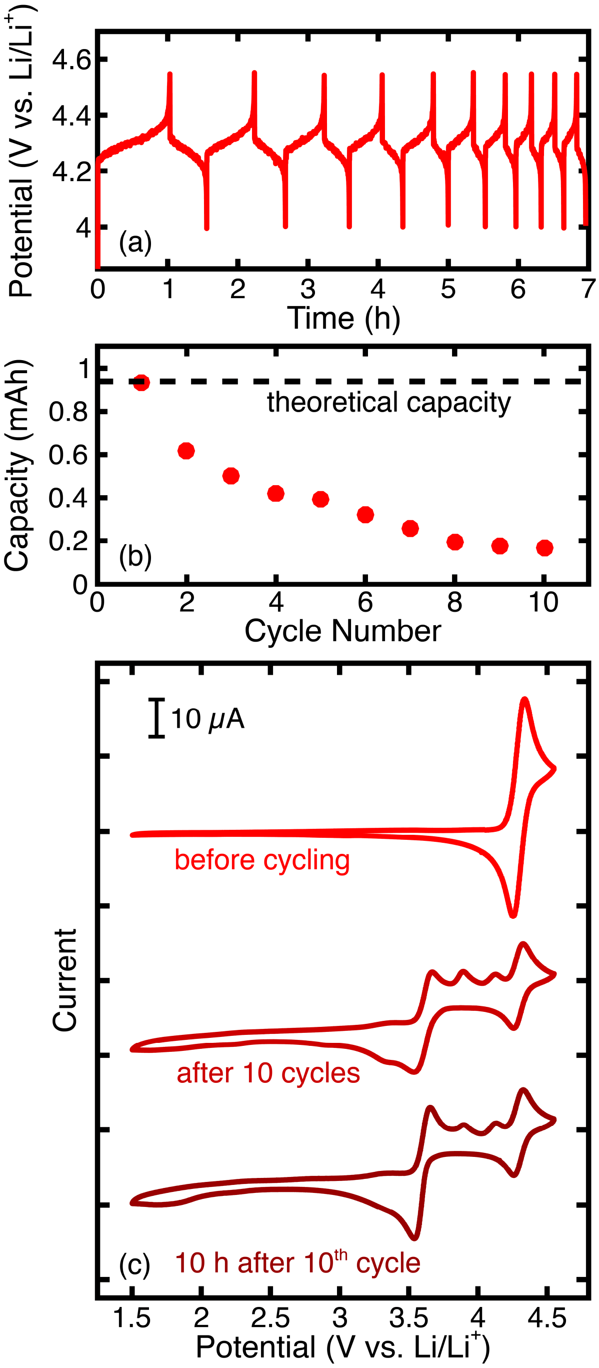

Figure 6: The voltage profiles of the first 10 cycles of 25FDB (a), and the corresponding capacity vs. cycle number profile (b). Cyclic voltammograms before cycling (top), immediately after 10 cycles (middle), and 10 h after 10 cycles (bottom) for 25FDB using a scan rate of 20 mV/s (c). The initial electrolyte composition was 0.010 M 25FDB in 1 M LiTFSI in PC. The working, counter, and reference electrodes used were a 3 mm glassy carbon disk, a RVC, and a fritted lithium foil, respectively. The applied current was 0.938 mA (1C) for both charge and discharge.

With every cycle, the peak current ratio associated with the redox potential of 25FDB remained constant, but the overall magnitude of the oxidative and reductive peak heights decreased indicating that the charged species decays, but does not negatively interact with the neutral species. Additionally, the decrease in the oxidative peak height of 25FDB generally tracks with the charging capacity accessed during cycling. As 25FDB is cycled, the voltammetry response evolves and becomes more complicated suggesting intricate decomposition processes and the formation of multiple electroactive decay intermediates and products. As expected, the magnitude of these newly formed peaks increased with cycle number indicating that, with further cycling, the decomposition continued. From the full set of voltammograms (Figure S19), a reduction peak at 3.379 V vs. Li/Li$^+$ appeared after the first cycle. After 25FDB is cycled further, 3 new oxidation peaks of similar magnitudes appeared at 3.653 V vs. Li/Li$^+$, 3.897 V vs. Li/Li$^+$, and 4.135 V vs. Li/Li$^+$. After cycle 5, a new reduction peak begins to form at 3.539 V vs. Li/Li$^+$, and the reduction peak at 3.379 V vs. Li/Li$^+$ starts to decrease in magnitude. The changes in the voltammogram profile and the current magnitudes as a function of cycle number indicate that 25FDB initially decays, but as the solution continues to cycle, these intermediates start to decay themselves, signifying a tiered mechanism. This is further evinced by comparing the voltammograms after 10 cycles and 10 h after completion of cycling. Even with no electrochemical stimulus applied to the solution, the voltammogram evolves, showing that the decomposition products are not stable on their own. As such, unambiguous identification of decay products is challenging due to the complexity of the electrochemical signal and NMR data. Thus, decomposition products could not be identified nor could a decomposition mechanism be confirmed. Previous work on substituted dialkoxybenzenes suggest that quinone and dimer formation are likely decay products [36,37,39]. Expanding upon these efforts, future work on halogenated species should aim to correlate possible decomposition products with the corresponding electrochemical and spectroscopy responses to confirm their presence. Once the decomposition products and the decay pathways are determined, the next generation of derivatives can be designed to be resilient to these failure modes but still enable increased redox potential [10,24,35].

Conclusions

This work investigates the effect of halidization on the dimethoxybenzene core using electrochemical techniques, NMR spectroscopy, and DFT calculations. Halidization is an effective method to increase the redox potential so that the oxidation occurs at or near the upper limit of the electrolyte stability window, potentially allowing for higher energy applications. Cyclic voltammetry was used to determine the redox potential, electrochemical reversibility, chemical reversibility, and the diffusion coefficient. With the exception of the iodide derivative, the increase in redox potential does not significantly affect the chemical reversibility at low concentrations on the CV timescale (~100 s).

Of the halide substitutions made, the fluorine derivative has many desirable properties as compared to the parent methyl compound. The fluorine groups increased the redox potential by about 360 mV, but only increased the molecular weight by 8 a.m.u compared to 25DDB. The fluorine groups also increased the solubility in the electrolytes used due to the additional polarity. However, the cyclability of this and other halide-substituted materials, is hampered by the limited charged state stability as the radical cation, which appears to decompose through scissioning of the carbon-halide bonds. While initial decay pathways were probed, the full decomposition mechanism could not be determined but appears complex and tiered. Further investigation of these mechanisms may inform molecular engineering of more robust derivatives which retain the high redox potentials of this initial set. While these halogen-substituted materials do not appear suitable for use as energy storage materials (e.g., active materials for redox flow batteries) as their limited charge state stability hampers cyclability, they may find use as part of a computational training set to guide the design of substituted dialkoxybenzenes with improved stability [24] or as redox mediators in electrochemical technologies including as overcharge protection additives in Li-ion batteries [17], as well as charge shuttles in dye-sensitized solar cells [58] and in flow batteries with solid materials in the tanks[59,60].

Acknowledgements

This work was supported as part of the Joint Center for Energy Storage Research, an Energy Innovation Hub funded by the U.S. Department of Energy, Office of Science, Basic Energy Sciences. We would also like to thank members of the energy storage subgroup in the Brushett group for helpful discussions and feedback.

References

[1] Z. Yang, J. Zhang, M.C.W. Kintner-Meyer, X. Lu, D. Choi, J.P. Lemmon, J. Liu, Electrochemical Energy Storage for Green Grid, Chem. Rev. 111 (2011) 3577–3613. doi:10.1021/cr100290v.
[2] S. Chu, A. Majumdar, Opportunities and challenges for a sustainable energy future, Nature. 488 (2012) 294–303. doi:10.1038/nature11475.
[3] Y.S. Chu, T.E. Lister, W.G. Cullen, H. You, Z. Nagy, others, Basic Reseach Needs for Electrical Energy Storage, (2007).
[4] A. Akhil, J. Boyes, P. Butler, Chapter 30: Batteries for electrical energy storage applications, in: Linden’s Handbook of Battery. Editor: T Reddy, 4th ed., McGraw-Hill, New York, 2010.
[5] International Energy Agency, Energy Technology Perspectives 2012: Pathways to a Clean Energy System, SourceOECD Energy. 2012 (2012) 1.
[6] M.L. Perry, A.Z. Weber, Advanced Redox-Flow Batteries: A Perspective, J. Electrochem. Soc. 163 (2016) A5064–A5067. doi:10.1149/2.0101601jes.

[7] J.A. Kowalski, L. Su, J.D. Milshtein, F.R. Brushett, Recent advances in molecular engineering of redox active organic molecules for nonaqueous flow batteries, Current Opinion in Chemical Engineering. 13 (2016) 45–52. doi:10.1016/j.coche.2016.08.002.

[8] D.-Y. Lee, M.-J. Lee, J.-W. Park, D.-J. Oh, J.-Y. Mun, S.-G. Doo, Aromatic ligand coordinated redox couples & their application into redox flow batteries, (2011).

[9] C.S. Sevov, S.K. Samaroo, M.S. Sanford, Cyclopropenium Salts as Cyclable, High-Potential Catholytes in Nonaqueous Media, Advanced Energy Materials. 7 (2017) 1602027. doi:10.1002/aenm.201602027.

[10] C.S. Sevov, R.E.M. Brooner, E. Chénard, R.S. Assary, J.S. Moore, J. Rodríguez-López, M.S. Sanford, Evolutionary Design of Low Molecular Weight Organic Anolyte Materials for Applications in Nonaqueous Redox Flow Batteries, J. Am. Chem. Soc. 137 (2015) 14465–14472. doi:10.1021/jacs.5b09572.

[11] J. Huang, L. Cheng, R.S. Assary, P. Wang, Z. Xue, A.K. Burrell, L.A. Curtiss, L. Zhang, Liquid Catholyte Molecules for Nonaqueous Redox Flow Batteries, Adv. Energy Mater. 5 (2015) n/a-n/a. doi:10.1002/aenm.201401782.

[12] J.A. Kowalski, M.D. Casselman, A.P. Kaur, J.D. Milshtein, C.F. Elliott, S. Modekrutti, N.H. Attanayake, N. Zhang, S.R. Parkin, C. Risko, F.R. Brushett, S.A. Odom, A stable two-electron-donating phenothiazine for application in nonaqueous redox flow batteries, J. Mater. Chem. A. 5 (2017) 24371–24379. doi:10.1039/C7TA05883G.

[13] C.G. Armstrong, K.E. Toghill, Stability of molecular radicals in organic non-aqueous redox flow batteries: A mini review, Electrochemistry Communications. 91 (2018) 19–24. doi:10.1016/j.elecom.2018.04.017.

[14] B. Huskinson, S. Nawar, M.R. Gerhardt, M.J. Aziz, Novel Quinone-Based Couples for Flow Batteries, ECS Trans. 53 (2013) 101–105. doi:10.1149/05307.0101ecst.

[15] J.D. Milshtein, L. Su, C. Liou, A.F. Badel, F.R. Brushett, Voltammetry study of quinoxaline in aqueous electrolytes, Electrochimica Acta. 180 (2015) 695–704. doi:10.1016/j.electacta.2015.07.063.

[16] C. Buhrmester, J. Chen, L. Moshurchak, J. Jiang, R.L. Wang, J.R. Dahn, Studies of Aromatic Redox Shuttle Additives for LiFePO4-Based Li-Ion Cells, J. Electrochem. Soc. 152 (2005) A2390–A2399. doi:10.1149/1.2098265.

[17] Z. Chen, Y. Qin, K. Amine, Redox shuttles for safer lithium-ion batteries, Electrochim. Acta. 54 (2009) 5605–5613. doi:10.1016/j.electacta.2009.05.017.

[18] C. Buhrmester, L.M. Moshurchak, R.L. Wang, J.R. Dahn, The Use of 2,2,6,6-Tetramethylpiperinyl-Oxides and Derivatives for Redox Shuttle Additives in Li-Ion Cells, J. Electrochem. Soc. 153 (2006) A1800–A1804. doi:10.1149/1.2221860.

[19] Z. Cai, Y. Liu, S. Liu, L. Li, Y. Zhang, High performance of lithium-ion polymer battery based on non-aqueous lithiated perfluorinated sulfonic ion-exchange membranes, Energy Environ. Sci. 5 (2012) 5690–5693. doi:10.1039/C1EE02708E.

[20] Y. Liang, Z. Tao, J. Chen, Organic Electrode Materials for Rechargeable Lithium Batteries, Adv. Energy Mater. 2 (2012) 742–769. doi:10.1002/aenm.201100795.

[21] Z. Song, H. Zhou, Towards sustainable and versatile energy storage devices: an overview of organic electrode materials, Energy Environ. Sci. 6 (2013) 2280. doi:10.1039/c3ee40709h.

[22] L. Cheng, R.S. Assary, X. Qu, A. Jain, S.P. Ong, N.N. Rajput, K. Persson, L.A. Curtiss, Accelerating Electrolyte Discovery for Energy Storage with High-Throughput Screening, J. Phys. Chem. Lett. 6 (2015) 283–291. doi:10.1021/jz502319n.

[23] C.W. Coley, R. Barzilay, T.S. Jaakkola, W.H. Green, K.F. Jensen, Prediction of Organic Reaction Outcomes Using Machine Learning, ACS Cent. Sci. 3 (2017) 434–443. doi:10.1021/acscentsci.7b00064.

[24] C.S. Sevov, D.P. Hickey, M.E. Cook, S.G. Robinson, S. Barnett, S.D. Minteer, M.S. Sigman, M.S. Sanford, Physical Organic Approach to Persistent, Cyclable, Low-Potential Electrolytes for Flow Battery Applications, J. Am. Chem. Soc. 139 (2017) 2924–2927. doi:10.1021/jacs.7b00147.

[25] J.D. Milshtein, J.L. Barton, R.M. Darling, F.R. Brushett, 4-acetamido-2,2,6,6-tetramethylpiperidine-1-oxyl as a model organic redox active compound for nonaqueous flow batteries, Journal of Power Sources. 327 (2016) 151–159. doi:10.1016/j.jpowsour.2016.06.125.

[26] X. Wei, W. Xu, M. Vijayakumar, L. Cosimbescu, T. Liu, V. Sprenkle, W. Wang, TEMPO-Based Catholyte for High-Energy Density Nonaqueous Redox Flow Batteries, Adv. Mater. 26 (2014) 7649–7653. doi:10.1002/adma.201403746.

[27] J.D. Milshtein, A.P. Kaur, M.D. Casselman, J.A. Kowalski, S. Modekrutti, P.L. Zhang, N.H. Attanayake, C.F. Elliott, S.R. Parkin, C. Risko, F.R. Brushett, S.A. Odom, High current density, long duration cycling of soluble organic active species for non-aqueous redox flow batteries, Energy Environ. Sci. (2016). doi:10.1039/C6EE02027E.

[28] L.M. Moshurchak, C. Buhrmester, R.L. Wang, J.R. Dahn, Comparative studies of three redox shuttle molecule classes for overcharge protection of LiFePO4-based Li-ion cells, Electrochimica Acta. 52 (2007) 3779–3784. doi:10.1016/j.electacta.2006.10.068.

[29] C. Buhrmester, L. Moshurchak, R.L. Wang, J.R. Dahn, Phenothiazine Molecules Possible Redox Shuttle Additives for Chemical Overcharge and Overdischarge Protection for Lithium-Ion Batteries, J. Electrochem. Soc. 153 (2006) A288–A294. doi:10.1149/1.2140615.

[30] M.D. Casselman, A.P. Kaur, K.A. Narayana, C.F. Elliott, C. Risko, S.A. Odom, The fate of phenothiazine-based redox shuttles in lithium-ion batteries, Phys. Chem. Chem. Phys. 17 (2015) 6905–6912. doi:10.1039/C5CP00199D.

[31] D.-H. Hwang, S.-K. Kim, M.-J. Park, J.-H. Lee, B.-W. Koo, I.-N. Kang, S.-H. Kim, T. Zyung, Conjugated Polymers Based on Phenothiazine and Fluorene in Light-Emitting Diodes and Field Effect Transistors, Chem. Mater. 16 (2004) 1298–1303. doi:10.1021/cm035264+.

[32] E.C. Montoto, Y. Cao, K. Hernández-Burgos, C.S. Sevov, M.N. Braten, B.A. Helms, J.S. Moore, J. Rodríguez-López, Effect of the Backbone Tether on the Electrochemical Properties of Soluble Cyclopropenium Redox-Active Polymers, Macromolecules. 51 (2018) 3539–3546. doi:10.1021/acs.macromol.8b00574.

[33] K.H. Hendriks, S.G. Robinson, M.N. Braten, C.S. Sevov, B.A. Helms, M.S. Sigman, S.D. Minteer, M.S. Sanford, High-Performance Oligomeric Catholytes for Effective Macromolecular Separation in Nonaqueous Redox Flow Batteries, ACS Cent. Sci. 4 (2018) 189–196. doi:10.1021/acscentsci.7b00544.

[34] J. Huang, L. Su, J.A. Kowalski, J.L. Barton, M. Ferrandon, A.K. Burrell, F.R. Brushett, L. Zhang, A subtractive approach to molecular engineering of dimethoxybenzene-based redox materials for non-aqueous flow batteries, J. Mater. Chem. A. 3 (2015) 14971–14976. doi:10.1039/C5TA02380G.

[35] J. Huang, B. Pan, W. Duan, X. Wei, R.S. Assary, L. Su, F.R. Brushett, L. Cheng, C. Liao, M.S. Ferrandon, W. Wang, Z. Zhang, A.K. Burrell, L.A. Curtiss, I.A. Shkrob, J.S. Moore,

L. Zhang, The lightest organic radical cation for charge storage in redox flow batteries, Scientific Reports. 6 (2016) 32102. doi:10.1038/srep32102.

[36] J. Zhang, Z. Yang, I.A. Shkrob, R.S. Assary, S. on Tung, B. Silcox, W. Duan, J. Zhang, C.C. Su, B. Hu, B. Pan, C. Liao, Z. Zhang, W. Wang, L.A. Curtiss, L.T. Thompson, X. Wei, L. Zhang, Annulated Dialkoxybenzenes as Catholyte Materials for Non-aqueous Redox Flow Batteries: Achieving High Chemical Stability through Bicyclic Substitution, Advanced Energy Materials. 7 (2017) 1701272. doi:10.1002/aenm.201701272.

[37] J. Zhang, I.A. Shkrob, R.S. Assary, S. on Tung, B. Silcox, L.A. Curtiss, L. Thompson, L. Zhang, Toward Improved Catholyte Materials for Redox Flow Batteries: What Controls Chemical Stability of Persistent Radical Cations?, J. Phys. Chem. C. 121 (2017) 23347–23358. doi:10.1021/acs.jpcc.7b08281.

[38] L. Zhang, Z. Zhang, P.C. Redfern, L.A. Curtiss, K. Amine, Molecular engineering towards safer lithium-ion batteries: a highly stable and compatible redox shuttle for overcharge protection, Energy Environ. Sci. 5 (2012) 8204–8207. doi:10.1039/C2EE21977H.

[39] J. Zhang, J. Huang, L.A. Robertson, I.A. Shkrob, L. Zhang, Comparing calendar and cycle life stability of redox active organic molecules for nonaqueous redox flow batteries, Journal of Power Sources. 397 (2018) 214–222. doi:10.1016/j.jpowsour.2018.07.001.

[40] X. Wei, W. Xu, J. Huang, L. Zhang, E. Walter, C. Lawrence, M. Vijayakumar, W.A. Henderson, T. Liu, L. Cosimbescu, B. Li, V. Sprenkle, W. Wang, Radical Compatibility with Nonaqueous Electrolytes and Its Impact on an All-Organic Redox Flow Battery, Angew. Chem. Int. Ed. 54 (2015) 8684–8687. doi:10.1002/anie.201501443.

[41] W. Duan, J. Huang, J.A. Kowalski, I.A. Shkrob, M. Vijayakumar, E. Walter, B. Pan, Z. Yang, J.D. Milshtein, B. Li, C. Liao, Z. Zhang, W. Wang, J. Liu, J.S. Moore, F.R. Brushett, L. Zhang, X. Wei, “Wine-Dark Sea” in an Organic Flow Battery: Storing Negative Charge in 2,1,3-Benzothiadiazole Radicals Leads to Improved Cyclability, ACS Energy Lett. 2 (2017) 1156–1161. doi:10.1021/acsenergylett.7b00261.

[42] F.R. Brushett, J.T. Vaughey, A.N. Jansen, An All-Organic Non-aqueous Lithium-Ion Redox Flow Battery, Adv. Energy Mater. 2 (2012) 1390–1396. doi:10.1002/aenm.201200322.

[43] S.M. Laramie, J.D. Milshtein, B.M. Bartlett, F.R. Brushett, L.T. Thompson, Performance and cost characteristics of multi-electron transfer, common ion exchange non-aqueous redox flow batteries, Journal of Power Sources. (Submitted). (n.d.).

[44] W.M. Haynes, CRC Handbook of Chemistry and Physics, 92nd Edition., CRC Press, Hoboken, 2011.

[45] F.L. Pilar, Rates and equilibria of organic reactions (Leffler, John E.; Grunwald, Ernest), J. Chem. Educ. 41 (1964) 407. doi:10.1021/ed041p407.1.

[46] C. Hansch, A. Leo, R.W. Taft, A survey of Hammett substituent constants and resonance and field parameters, Chem. Rev. 91 (1991) 165–195. doi:10.1021/cr00002a004.

[47] E.V. Carino, J. Staszak-Jirkovsky, R.S. Assary, L.A. Curtiss, N.M. Markovic, F.R. Brushett, Tuning the Stability of Organic Active Materials for Nonaqueous Redox Flow Batteries via Reversible, Electrochemically Mediated Li+ Coordination, Chem. Mater. 28 (2016) 2529–2539. doi:10.1021/acs.chemmater.5b04053.

[48] J.E. Bachman, L.A. Curtiss, R.S. Assary, Investigation of the Redox Chemistry of Anthraquinone Derivatives Using Density Functional Theory, J. Phys. Chem. A. (2014). doi:10.1021/jp5060777.

[49] W.M. Deen, Analysis of Transport Phenomena, Topics in Chemical Engineering, Oxford University Press, New York, 1998.

[50] J. Zhang, R.E. Corman, J.K. Schuh, R.H. Ewoldt, I.A. Shkrob, L. Zhang, Solution Properties and Practical Limits of Concentrated Electrolytes for Nonaqueous Redox Flow Batteries, J. Phys. Chem. C. 122 (2018) 8159–8172. doi:10.1021/acs.jpcc.8b02009.

[51] H. Fujita, A. Kishimoto, K. Matsumoto, Concentration and temperature dependence of diffusion coefficients for systems polymethyl acrylate and n-alkyl acetates, Transactions of the Faraday Society. 56 (1960) 424–437.

[52] L. Su, M. Ferrandon, J.A. Kowalski, J.T. Vaughey, F.R. Brushett, Electrolyte Development for Non-Aqueous Redox Flow Batteries Using a High-Throughput Screening Platform, J. Electrochem. Soc. 161 (2014) A1905–A1914. doi:10.1149/2.0811412jes.

[53] L. Su, M. Ferrandon, J.L. Barton, N.U. de la Rosa, J.T. Vaughey, F.R. Brushett, An investigation of 2,5-di-tertbutyl-1,4-bis(methoxyethoxy)benzene in ether-based electrolytes, Electrochimica Acta. 246 (2017) 251–258. doi:10.1016/j.electacta.2017.05.167.

[54] E. Kissa, Fluorinated surfactants and repellents, CRC Press, 2001.

[55] Z. Chen, K. Amine, Degradation pathway of 2,5-di-tert-butyl-1,4-dimethoxybenzene at high potential, Electrochimica Acta. 53 (2007) 453–458. doi:10.1016/j.electacta.2007.06.073.

[56] T. Li, L. Xing, W. Li, B. Peng, M. Xu, F. Gu, S. Hu, Theoretic Calculation for Understanding the Oxidation Process of 1,4-Dimethoxybenzene-Based Compounds as Redox Shuttles for Overcharge Protection of Lithium Ion Batteries, The Journal of Physical Chemistry A. 115 (2011) 4988–4994. doi:10.1021/jp2004584.

[57] J. Jones, M. Anouti, M. Caillon-Caravanier, P. Willmann, P.-Y. Sizaret, D. Lemordant, Solubilization of SEI lithium salts in alkylcarbonate solvents, Fluid Phase Equilibria. 305 (2011) 121–126. doi:10.1016/j.fluid.2011.03.007.

[58] T. W. Hamann, R. A. Jensen, A.B. F. Martinson, H.V. Ryswyk, J. T. Hupp, Advancing beyond current generation dye -sensitized solar cells, Energy & Environmental Science. 1 (2008) 66–78. doi:10.1039/B809672D.

[59] Q. Wang, S.M. Zakeeruddin, D. Wang, I. Exnar, M. Grätzel, Redox Targeting of Insulating Electrode Materials: A New Approach to High-Energy-Density Batteries, Angewandte Chemie International Edition. 45 (2006) 8197–8200. doi:10.1002/anie.200602891.

[60] Q. Huang, H. Li, M. Grätzel, Q. Wang, Reversible chemical delithiation/lithiation of LiFePO 4 : towards a redox flow lithium-ion battery, Physical Chemistry Chemical Physics. 15 (2013) 1793–1797. doi:10.1039/C2CP44466F.

TOC Figure

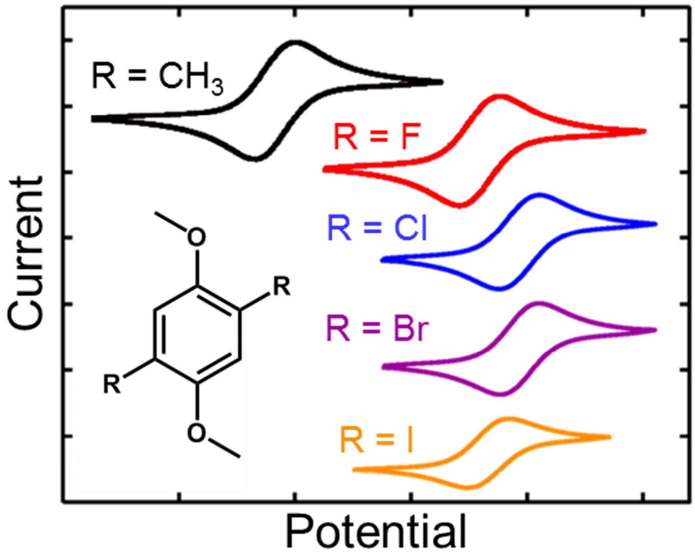

Table 1: A summary of electrochemical and transport properties of 25DDB, 25FDB, 25CIDB, 25BrDB, and 25IDB as determined from CV experiments performed in 1.0 M LiTFSI in PC (top) and 1.0 M LiTFSI in DME (*bottom*), and the ionization potential determined by DFT. All electrochemical experiments were performed in triplicate.

	25DDB	25FDB	25ClDB	25BrDB	25IDB
Redox Potential (V vs. Li/Li$^+$)	3.930 ± 0.001 *3.964 ±0.001*	4.301 ± 0.001 *4.318 ±0.001*	4.359 ± 0.001 *4.386 ±0.001*	4.361 ± 0.001 *4.388 ±0.001*	— *4.332 ±0.001*
Ionization Potential (eV)	5.447	5.643	5.663	5.654	—
Peak Separation (mV)	60.3 ± 0.7 *62.2 ±0.3*	61.0 ± 0.6 *60.3 ±0.3*	61 ± 1 *62.7 ±0.9*	61.7 ± 0.9 *65 ±2*	— *80 ±5*
Peak Current Ratio ($I_{p,o}$ / $I_{p,r}$)	1.003 ± 0.002 *1.01 ± 0.01*	1.03 ± 0.01 *1.01 ± 0.01*	1.04 ± 0.02 *1.05 ± 0.01*	1.08 ± 0.03 *1.06 ± 0.03*	— *1.17 ± 0.05*
Diffusivity (× 10^{-6} cm^2/s)	2.4 ± 0.1 *12.0 ±0.4*	1.6 ± 0.1 *8.6 ±0.9*	1.4 ± 0.1 *7.6 ±0.2*	1.3 ± 0.1 *7.1 ±0.1*	— *5.5 ±0.2*

Table 2: A summary of physical properties of 25DDB, 25FDB, 25ClDB, 25BrDB, and 25IDB in 1 M LiTFSI in PC (top) and 1 M LiTFSI in DME (*bottom*).

	25DDB	25FDB	25ClDB	25BrDB	25IDB
Molecular Diameter (Å)	9.1	8.4	9.7	10.2	11.0
Effective Solvated Diameter (Å)	21 ± 1 *28 ±1*	32 ± 1 *40 ±4*	36 ± 2 *44 ±1*	41 ± 2 *48 ±1*	— *62 ±2*
Solubility (mol/L)	0.10 *0.35*	0.19 *0.42*	0.10 *0.27*	0.05 *0.18*	Insol. *0.03*

Table 3: Summary of the major NMR peaks before and after cycling. Note that the solvent and supporting salt peaks are omitted from this table (See Figure S17 and Figure S18 for background NMR scans).

	^{1}H NMR	^{19}F NMR
Before cycling	3.55 (s), 7.06 (dd) J = 10.5	-138.7 (t) J = 10.1
After cycling	3.19 (s), 3.47 (s), 4.48 (s), 5.93 (s)	None

Declaration of interests

☒ The authors declare that they have no known competing financial interests or personal relationships that could have appeared to influence the work reported in this paper.

☐The authors declare the following financial interests/personal relationships which may be considered as potential competing interests: